Supporting Information

Tailoring the Porosity and Microstructure of Printed Graphene Electrodes via Polymer Phase Inversion

Ethan B. Secor[†,‡], *Manuel H. Dos Santos*[†], *Shay G. Wallace*[†], *Nathan P. Bradshaw*[†], *and Mark C. Hersam*[†, §, *]

† Department of Materials Science and Engineering, Northwestern University, Evanston, IL 60208, United States

§ Department of Chemistry, Department of Electrical Engineering and Computer Science, Northwestern University, Evanston, IL 60208, United States

‡ Present address: Sandia National Laboratories, Albuquerque, NM 87185, United States

* Corresponding Author: m-hersam@northwestern.edu

Experimental Methods

Liquid-phase exfoliation and processing of graphene. Graphene exfoliation was performed using a high shear mixer with graphite, ethyl cellulose, and ethanol, as reported previously.[1,2] Ethyl cellulose (4 cP grade, Sigma Aldrich) was added to ethanol (200 proof) at a concentration of 20 mg/mL, followed by the addition of flake graphite (Asbury Graphite Mills, Grade 3061) at a concentration of 300 mg/mL. This mixture was processed with a high shear mixer, using cooling water to maintain the mixture at room temperature. The resulting mixture was centrifuged to remove unexfoliated graphite flakes at 5,000 rpm for 20 minutes (Beckman Coulter Avanti J-26 XPI centrifuge). The supernatant was collected and mixed with salt water (0.04 g/mL NaCl, Fisher BioReagents, in deionized water) in a ratio of ~16:9 w/w, and then centrifuged at 6,000 rpm for 6 minutes to sediment the graphene/EC composite. This composite was washed with deionized water and dried to yield a fine black powder containing graphene and EC, with ~40% wt. graphene.

Ink formulation and printing. Graphene/EC powder, nitrocellulose powder (NC, Scientific Polymer, Cat. #714), glycerol, and ethyl lactate were directly mixed to prepare inks using bath sonication. For direct ink writing, a Hyrel System 30M 3D printer was used, with a 210 μm diameter extrusion tip. For multilayer printing, the print bed was held at 60 °C to accelerate drying. Glass substrates were cleaned with ethanol prior to printing. It should be noted that nitrocellulose with high nitrogen content is highly reactive, and thus care should be taken in handling the material to mitigate risks.

Phase inversion process flow. Samples were cast by stencil printing or direct ink writing, and dried at 70 °C for 10 minutes to remove the ethyl lactate primary solvent. For standard processing, a vacuum drying step at 100 °C for 10 hours was employed to remove the glycerol nonsolvent. Alternatively, the partially-dried films could be immersed in deionized water to leach out glycerol, following by drying at 70 °C for 10 minutes to remove residual water. Finally, the samples were annealed on a hotplate at 325 °C for 30 minutes to partially decompose the polymer dispersants.

Chemical and structural characterization. All electrical measurements were collected using a Keithley source meter. Film samples were characterized using an in-line four point probe measurement system, taking into account appropriate geometric correction factors. Raman spectra were obtained using a Horiba Xplora Raman microscope equipped with a 532 nm laser. Peak intensity ratios indicate the average and standard deviation of 3 different spectra collected at different locations. Note that a low laser power and long integration time were employed to reduce local heating, although some evidence of heating was still observed for the more porous samples. Scanning electron microscopy (SEM) images were collected using a Hitachi SU8030 SEM without any additional conductive coating.

Microsupercapacitor fabrication and testing. For microsupercapacitor fabrication, a Hyrel 3D System 30M printer was used to print graphene interdigitated electrodes. Following electrode processing and annealing, a gel electrolyte was applied that contained 1.0 g phosphoric acid, 1.0 g

PVA (M_w = 50,000, Aldrich), 3.0 g isopropyl alcohol, and 6.0 g water, similar to that reported previously.[3] The samples were then dried overnight and tested by cyclic voltammetry and chronopotentiometry using a CHI 760D potentiostat.

Ink Design: Phase Inversion without Nitrocellulose

As noted in the text, nitrocellulose is added to the graphene/ethyl cellulose ink to enhance gelation and phase inversion. Initial experiments did not include this addition of nitrocellulose, and led to inconsistent results. Notably, it was observed that the graphene films could collapse and yield a denser microstructure, even with up to 12.5% glycerol, leading to inhomogeneity in the film, as shown in Figure S1. As a result, nitrocellulose was added for all experiments discussed in the main text because its strong hydrophobic nature enhances the phase inversion process.

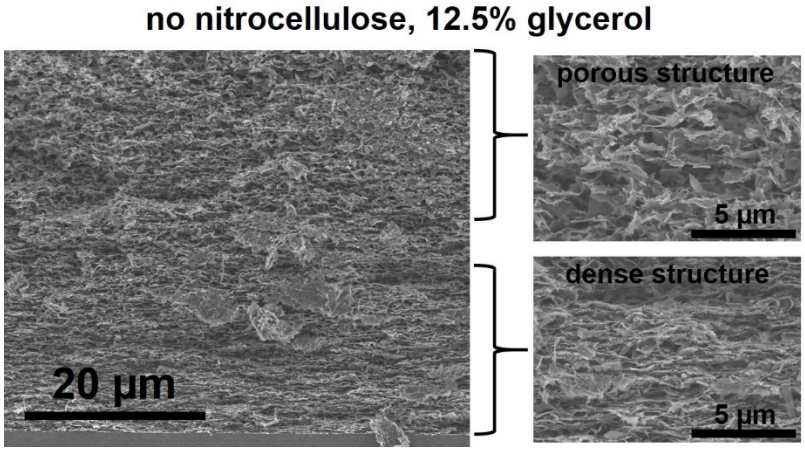

Figure S1. Cross-sectional SEM image of a graphene/ethyl cellulose film, following phase inversion with 12.5% glycerol. It is noted that, while the top portion of the film shows characteristic microstructural features of effective phase inversion, the bottom section exhibits a dense microstructure. Nitrocellulose was added to subsequent inks to prevent this inhomogeneity and inconsistency in the process.

FTIR Spectroscopy

Fourier transform infrared spectroscopy was performed to confirm that glycerol is effectively removed from the films during the vacuum drying step. Representative spectra for inks with 0, 5, 10, and 15% glycerol are shown in Figure S2. Residual glycerol would likely result in a prominent -OH peak above 3000 cm^{-1}, but no peaks in this region of the spectra are evident.

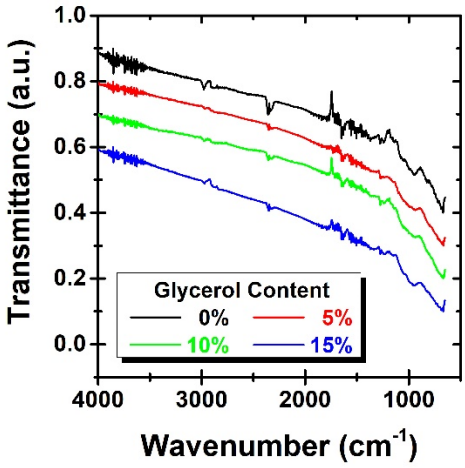

Figure S2. FTIR spectroscopy characterization for samples from each ink, showing similar spectra following vacuum drying. Transmittance values are scaled and shifted for easier comparison between the samples.

Porosity Estimation

The design of the experiment allows direct comparison between the volume of films prepared from each ink. In particular, the ink solids loading is equivalent in each case, and the wet film thickness is, to first order, determined by the stencil thickness. Therefore, the dry film thickness can be used to gauge density and porosity. Using a density value for comparable graphene films prepared without phase inversion of 1.12 g/cm^3,[3] porosity values for films derived from 0, 5, 10, and 15% glycerol containing inks were estimated to be 0.51±0.05, 0.74±0.02, 0.81±0.03, and 0.92±0.01, as shown in Figure S3.

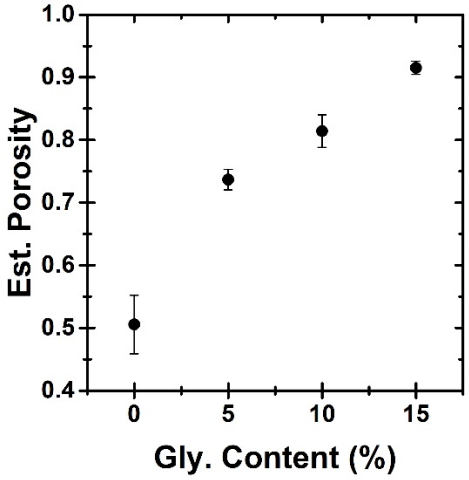

Figure S3. Estimated porosity for different graphene films based on the film thickness measurements.

Raman Spectroscopy

Raman spectroscopy was performed to confirm that the phase inversion processing methods do not chemically alter the graphene film. Representative spectra for inks with 0, 5, 10, and 15% glycerol are shown in Figure S4a. There appears to be a slight decrease in the D peak for the 15% glycerol film, likely resulting from laser heating during the measurement coupled with the poor heat transfer through the highly porous film. Figure S4b shows the summary of I_D/I_G and the G peak position for each sample. Indeed, while the I_D/I_G is somewhat lower for the 15% film, the G peak position is shifted, indicative of heating.

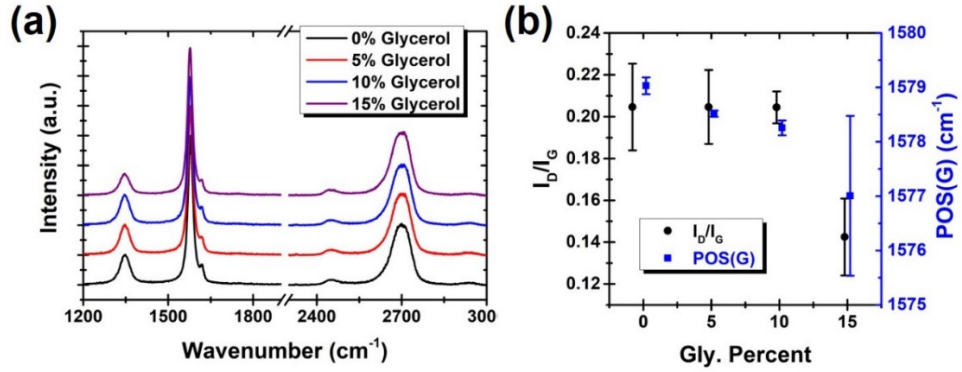

Figure S4. Raman spectroscopy characterization. (a) Representative spectra for graphene films with 0, 5, 10, and 15% glycerol (collected following all processing steps, including thermal annealing). (b) Summary of peak intensity ratio and G peak position for the four samples.

Control Samples for Printed Films

To confirm that the direct ink writing process does not interfere with successful phase inversion, inks with 0% and 10% glycerol were printed and compared. As shown in Figure S5, the two inks yield features with markedly different thicknesses and cross sectional areas, indicating that the phase inversion process is maintained for this deposition technique.

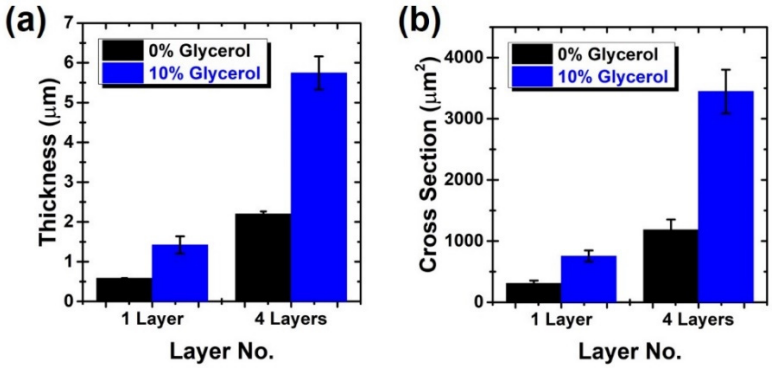

Figure S5. (a) Thickness and (b) cross sectional area for printed lines using the inks with 0% and 10% glycerol. The significantly higher values observed for the phase inversion ink with 10% glycerol indicate that the method is robust and not likely affected by the printing process.

Additional Supercapacitor Characterization

To determine a suitable ink formulation for testing microsupercapacitors, standard sandwich-structured supercapacitors were fabricated by stencil printing to compare the phase inversion inks. Charge/discharge cycling of these supercapacitors was performed to calculate the device capacitance as a function of current density, shown in Figure S6. At low current density, the 15% glycerol ink yields the highest capacitance, consistent with its high porosity. However, at higher current densities, the improved conductivity resulting from the 5% glycerol ink leads to the best rate capability. Due to this tradeoff, the 10% glycerol ink was chosen for microsupercapacitor fabrication, as it exhibits high capacitance at low current density along with suitable rate capability.

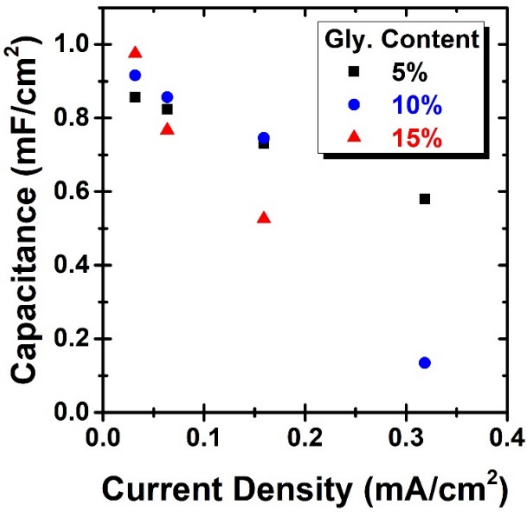

Figure S6. Capacitance plotted against current density for supercapacitors fabricated from phase inversion inks with 5, 10, and 15% glycerol. Sandwich-structured devices are used for a better comparison based on the amount of active material. At low current density, the more porous structure resulting from a high glycerol content leads to a higher capacitance. However, the lower electrical conductivity limits the rate capability of these devices. The ink with 10% glycerol was used for microsupercapacitors with a balance of high capacitance and rate capability.

The data from charge/discharge cycling of microsupercapacitors are used to calculate the energy and power densities of the devices, which are shown in Figure S7a for 1-layer and 4-layer devices. These values are higher than those observed for similar graphene microsupercapacitors based on graphene/ethyl cellulose and graphene/nitrocellulose,[4] indicating the benefit of the phase inversion process for increasing the active surface area (Figure S7b). The values for areal capacitance are highly competitive with printed graphene-based microsupercapacitors in the literature. In particular, Li *et al.* recently reported a record value of ~0.57 mF/cm^2 at a current of 0.02 mA/cm^2 for printed graphene microsupercapacitors, which is a lower current and capacitance than that reported here.[5]

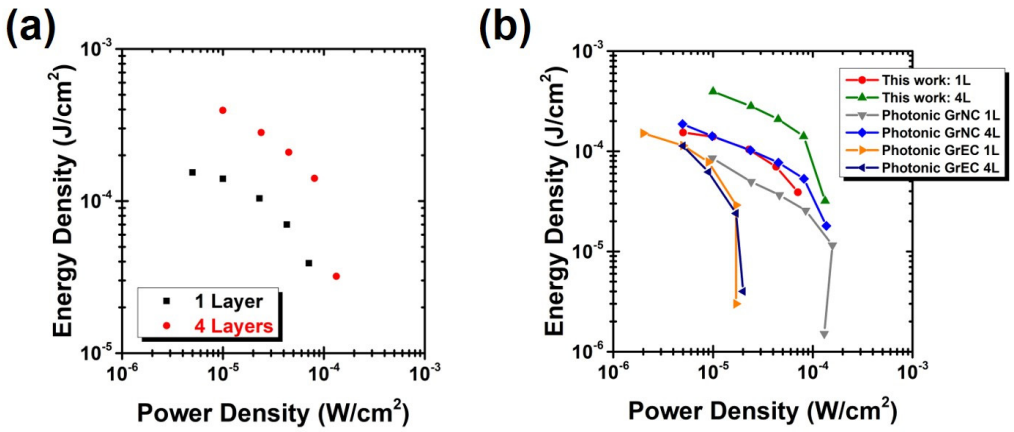

Figure S7. Ragone plots of energy density versus power density for the 1-layer and 4-layer devices tested here (a) and for these devices compared to prior data for similar inks without phase inversion processing (b).

References

(1) Secor, E. B.; Prabhumirashi, P. L.; Puntambekar, K.; Geier, M. L.; Hersam, M. C. Inkjet Printing of High Conductivity, Flexible Graphene Patterns. *J. Phys. Chem. Lett.* **2013**, *4*, 1347–1351.

(2) Secor, E. B.; Ahn, B. Y.; Gao, T. Z.; Lewis, J. A.; Hersam, M. C. Rapid and Versatile Photonic Annealing of Graphene Inks for Flexible Printed Electronics. *Adv. Mater.* **2015**, *27*, 6683–6688.

(3) Li, L.; Secor, E. B.; Chen, K.; Zhu, J.; Liu, X.; Gao, T. Z.; Seo, J. T.; Zhao, Y.; Hersam, M. C. High-Performance Solid-State Supercapacitors and Microsupercapacitors Derived from Printable Graphene Inks. *Adv. Energy Mater.* **2016**, *6*, 1600909.

(4) Secor, E. B.; Gao, T. Z.; Santos, M. H. Dos; Wallace, S. G.; Putz, K. W.; Hersam, M. C. Combustion-Assisted Photonic Annealing of Printable Graphene Inks via Exothermic Binders. *ACS Appl. Mater. Interfaces* **2017**, *9*, 29418–29423.

(5) Li, J.; Sollami Delekta, S.; Zhang, P.; Yang, S.; Lohe, M. R.; Zhuang, X.; Feng, X.; Östling, M. Scalable Fabrication and Integration of Graphene Microsupercapacitors through Full Inkjet Printing. *ACS Nano* **2017**, *11*, 8249–8256.